Paper

A Thermal Model of a Forced-Cooled Heat Sink for Transient Temperature Calculations Employing a Circuit Simulator

Uwe Drofenik* Non-member
Johann W. Kolar* Member

Power semiconductors can be modeled as a thermal network of resistors and capacitors. The thermal boundary condition of such a model is typically defined as the heat sink surface temperature, which is assumed to be constant. In reality, the heat sink surface temperature underneath the power module is not exactly known. In this paper we show how to set up a thermal model of the heat sink in form of a RC thermal equivalent network that can be directly embedded in any circuit simulator. The proposed thermal heat sink model takes into account convection cooling, thermal hotspots on the heat sink base plate, thermal time constants of the heat sink, and thermal coupling between different power modules mounted onto the heat sink. Experimental results are given and show high accuracy of the heat sink model with temperature errors below 10%.

Keywords: heat sink, dynamic thermal model, thermal coupling, thermal hot spot, heat transfer coefficient

1. Introduction

1.1 Thermal Simulations Employing a Circuit Simulator In order to optimize system design concerning increasing power density and reliability issues, there is a need to be able to perform, besides numerical circuit simulation, stationary and coupled transient numerical thermal simulations. Generally, a power module and its internal semiconductors can be set up, in good approximation, as a thermal network consisting of thermal resistors and capacitors. Such thermal models can be directly built into any circuit simulator with minimum effort. The circuit simulator estimates the semiconductor losses, and the time behavior of the losses is coupled with the thermal model resulting in the time behavior of the junction temperature Ref. (1), (2). The thermal boundary condition of such a thermal semiconductor model is typically defined as the heat sink surface temperature which is assumed to be constant.

On the international stage, there is work undertaken to implement thermo-electrical simulations of complex converter systems via finite element (3D-FEM) simulations embedded in circuit simulations, e.g. Ref. (3) and (4), which is very time-intensive. To increase computational efficiency, there are research efforts to implement parts of the system (e.g. cooling system) by employing stationary 3D-FEM simulations, and extract boundary condition information for other parts of the system (e.g. power module), Ref. (5)–(8). While a lot of work has been performed concerning the thermal modeling of the power semiconductor and/or the power module (e.g. Ref. (9)–(17)), heat sink models to be employed in circuit simulators are not common in power electronics, although the temperature-drop from heat sink to ambient might easily be in the range of the junction-case temperature drop. For example, in Ref. (18), a heat sink model for circuit simulators has been proposed based on the finite difference method, but it does not describe how to get the heat transfer coefficient characterizing convection cooling, as compared to the procedure proposed in this paper.

1.2 Defining a Thermal Model of the Heat Sink
Setting up a simple thermal model of a heat sink suitable for embedding it in a circuit simulation considering
- thermal hotspots
- thermal coupling between neighboring power modules
- dynamic behavior (time constants of the heat sink)
- convection cooling

is difficult because of the complex fin geometry, the three-dimensional temperature distribution, the impact of the fan characteristics and the often complex and difficult-to-model environment of the heat sink within a system environment. Furthermore, the transient thermal impedance (and/or thermal resistance) of the heat sink as experienced from the viewpoint of a power module, is strongly dependent on the size and location of this power module mounted onto the heat sink.

In this paper we propose a method for setting up a heat sink model considering all effects listed above. The procedure works as follows:
- Take a heat sink plus fan and mount a rectangular test heat source onto the center of the heat sink base plate.
- Heat up the configuration and measure the stationary temperature at a base plate point close to the test source.
- Use geometry, material parameters, and the measured temperature to parameterize the equations as given.
- Describe the location and size of the power modules to be placed on the heat sink for the final system design.
- Employ analytical equations and numerical finite-difference calculations (no computational fluid dynamics (CFD) needed!) as described.
- Get a RC thermal equivalent circuit of the heat sink to

* Power Electronic Systems Laboratory (PES), ETH Zurich
ETH-Zentrum/ETL H13, CH-8092 Zurich, Switzerland
drofenik@lem.ee.ethz.ch, kolar@lem.ee.ethz.ch, www.pes.ee.ethz.ch

be employing in a circuit simulator.

Based on a very simple stationary temperature measurement an easy-to-use heat sink model can be derived. The necessary calculations include a transient numerical simulation of the temperature distribution inside a 3D-rectangular block of homogenous material which can be done with software based on the finite element method (FEM) employing only the heat conduction equation, but also with quite simple self-written finite difference code (FDM).

Compared to otherwise necessary CFD-simulations of the heat sink including the air-flow, simulation times on today's (2004/05) PCs are reduced from a few hours to less than one minute. Furthermore, CFD simulations of heat sinks with a large number of fins tend to be numerically unstable and often show weak convergence, while the FEM-simulations as employed for the thermal models introduced in this paper show excellent numerical stability.

First, we have to find the heat transfer coefficient of the air-cooled heat sink based on a base plate surface temperature measurement (section 2). This heat transfer coefficient is essential to set up a simplified thermal model of the heat sink. In section 3, the simplified thermal model will be employed to numerically calculate thermal step responses. This will be compared to two experimental setups. In section 4, a RC thermal equivalent circuit of the heat sink will be extracted from the calculated step responses.

2. Heat Transfer Coefficient of an Air-Cooled Heat Sink

2.1 Finding the Heat Transfer Coefficient of a Heat Sink The heat sink temperature is defined by convective cooling which can be generally described by a heat transfer coefficient $h\,[\mathrm{W/m^2K}]$ defined according to

$$Q = A \cdot h \cdot \Delta T \quad \cdots\cdots (1)$$

with the thermal power Q [W], the total surface area (mainly provided by the fins) exposed to convection cooling $A\,[\mathrm{m^2}]$, and the temperature drop from fin surface to ambient ΔT [°C]. In case of forced convection (which is the focus of this paper) the heat transfer coefficient h is strongly dependent on fan characteristic and air flow inside the cabinet of the power electronic system. The proposed modeling procedure is based on the assumption that the heat flow from the fins into the air can be described in good approximation by a constant heat transfer coefficient h = const.

As shown in Ref. (19), the three-dimensional temperature field $T(x, y, z)$ of a plate with a rectangular heat source located at the center (Fig. 1) together with a Neumann boundary condition (characterized by a heat transfer coefficient h = const) at the bottom side $z = d$ and thermal isolation ($h = 0$) at all other surfaces, can by described (by analytically solving the three-dimensional heat conduction differential equation via Fourier series) as

$$\begin{aligned} T(x,y,z,h) &= T_a + \tfrac{1}{4}\psi_{00}(z,h) \\ &+ \sum_{l=1}^{\infty} \tfrac{1}{2}\psi_{l0}(z,h)\cos(\tfrac{l\pi x}{a}) + \sum_{m=1}^{\infty} \tfrac{1}{2}\psi_{0m}(z,h)\cos(\tfrac{m\pi y}{b}) \\ &+ \sum_{l=1}^{\infty}\sum_{m=1}^{\infty} \psi_{lm}(z,h)\cos(\tfrac{l\pi x}{a})\cos(\tfrac{m\pi y}{b}) \quad \cdots\cdots (2) \end{aligned}$$

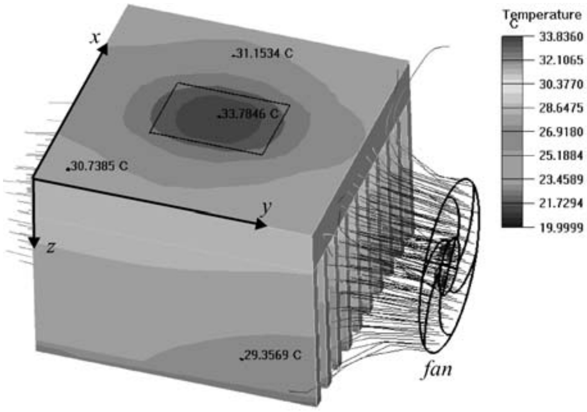

(a)

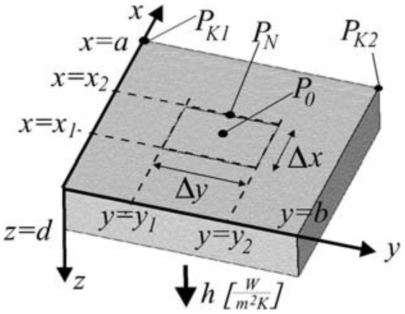

(b)

Fig. 1. (a) A CFD simulation shows the temperature field and air flow for a heat sink. In the vicinity of the power module there is a hot spot. (b) The simplified heat sink model consists of a plate with a heat transfer coefficient h = const as boundary condition at the bottom side, and thermal isolation (h = 0) at all other surfaces.

$h\,[\mathrm{W/m^2K}]$	...heat transfer coefficient
Q [W]	...thermal power
T_a [°C]	...ambient temperature
k [W/mK]	...thermal conductivity of heat sink material
x, y, z [m]	...Cartesian coordinates as defined in Fig. 1(b)
a, b, d [m]	...plate dimensions (Fig. 1(b))
x_1, x_2, y_1, y_2 [m]	...heat source dimensions (Fig. 1(b))
$\Delta x = x_2 - x_1, \Delta y = y_2 - y_1$	...heat source dimensions

with the coefficients

$$\psi_{00}(z,h) = \frac{4Q}{kab}\cdot\left(d + \tfrac{k}{h} - z\right) \quad \cdots\cdots (3)$$

$$\psi_{l0}(z,h) = \frac{8Qa}{\pi^2 b l^2 k \Delta x}\cdot\sin\left(\tfrac{l\pi(x_2-x_1)}{2a}\right)\cdot\cos\left(\tfrac{l\pi(x_2+x_1)}{2a}\right) \cdot\frac{\cosh\left(\frac{l\pi(z-d)}{a}\right) - \left(\frac{ha}{l\pi k}\right)\cdot\sinh\left(\frac{l\pi(z-d)}{a}\right)}{\sinh\left(\frac{l\pi d}{a}\right) + \left(\frac{ha}{l\pi k}\right)\cdot\cosh\left(\frac{l\pi d}{a}\right)} \quad \cdots\cdots (4)$$

$$\psi_{0m}(z,h) = \frac{8Qb}{\pi^2 a m^2 k \Delta y}\cdot\sin\left(\tfrac{m\pi(y_2-y_1)}{2b}\right)\cdot\cos\left(\tfrac{m\pi(y_2+y_1)}{2b}\right) \cdot\frac{\cosh\left(\frac{m\pi(z-d)}{b}\right) - \left(\frac{hb}{m\pi k}\right)\cdot\sinh\left(\frac{m\pi(z-d)}{b}\right)}{\sinh\left(\frac{m\pi d}{b}\right) + \left(\frac{hb}{m\pi k}\right)\cdot\cosh\left(\frac{m\pi d}{b}\right)} \quad \cdots\cdots (5)$$

$$\psi_{lm}(z,h) = \frac{16Q}{\pi^2 lmk\Delta x\Delta y}\cdot\sin\left(\tfrac{l\pi(x_2-x_1)}{2a}\right)\cdot\cos\left(\tfrac{l\pi(x_2+x_1)}{2a}\right) \cdot\sin\left(\tfrac{m\pi(y_2-y_1)}{2b}\right)\cdot\cos\left(\tfrac{m\pi(y_2+y_1)}{2b}\right)\cdot\frac{M}{N_1\cdot N_2} \quad \cdots\cdots (6)$$

$$M = \cosh\left((z-d)\sqrt{\left(\tfrac{l\pi}{a}\right)^2 + \left(\tfrac{m\pi}{b}\right)^2}\right)$$

$$-\left(\frac{k}{h}\sqrt{\left(\frac{l\pi}{a}\right)^2+\left(\frac{m\pi}{b}\right)^2}\right)^{-1}\cdot\sinh\left((z-d)\sqrt{\left(\frac{l\pi}{a}\right)^2+\left(\frac{m\pi}{b}\right)^2}\right) \quad \cdots\cdots\cdots\cdots (7)$$

$$N_1=\cosh\left(d\sqrt{\left(\frac{l\pi}{a}\right)^2+\left(\frac{m\pi}{b}\right)^2}\right)+\left(\frac{k}{h}\sqrt{\left(\frac{l\pi}{a}\right)^2+\left(\frac{m\pi}{b}\right)^2}\right)^{-1}\cdot\sinh\left(d\sqrt{\left(\frac{l\pi}{a}\right)^2+\left(\frac{m\pi}{b}\right)^2}\right) \quad \cdots\cdots\cdots\cdots (8)$$

$$N_2=\sqrt{\left(\frac{l\pi}{a}\right)^2+\left(\frac{m\pi}{b}\right)^2} \quad \cdots\cdots\cdots\cdots (9)$$

Equations (2)–(9) can be easily implemented in any programming language, and the number of coefficients is dependent on the geometry ratios $\Delta x/a$ and/or $\Delta y/b$. The smaller, e.g., Δx compared to a, the more Fourier coefficients are necessary to describe the power module geometry accurately. For details see Ref. (19).

If the temperature at a point at the heat sink surface, e.g. P_N in Fig. 1, is known, the heat transfer coefficient h of the air-cooled heat sink can be calculated from (10) which is directly derived from (2).

$$T_{PN}=T(x=x_2, y=b/2, z=0, h)=T(h) \quad \cdots\cdots (10)$$

This can be done, for example, graphically for a certain power module ($\Delta x/a = 0.214$) as shown in Fig. 2. First, based on (2)–(9) and/or (10) the temperature at a certain point is plotted dependent on a varying heat transfer coefficient h. In Fig. 2 and/or (10) this is done for point P_N close to the power module as shown in Fig. 1, where a temperature sensor can be easily placed. In this example, the temperature at point P_N is derived via a stationary CFD simulation of the heat sink shown in Fig. 1. With $T_{PN} = 50.78°\mathrm{C}$ at ambient temperature $T_a = 40°\mathrm{C}$, the heat transfer coefficient be found for this certain "heat sink plus fan"—configuration as $h = 524\,\mathrm{W/m^2K}$.

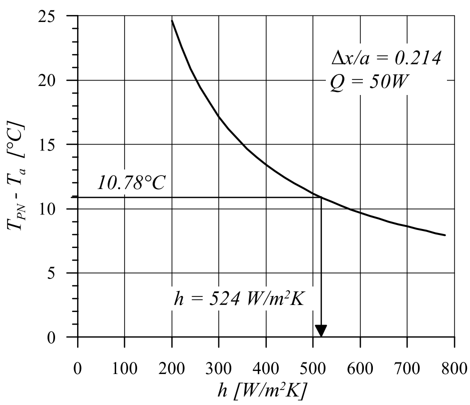

Fig. 2. Dependency of the temperature at surface point P_N on the heat transfer coefficient $h\,[\mathrm{W/m^2K}]$ for an air-cooled heat sink ($a = 112\,\mathrm{mm}$, $b = 100\,\mathrm{mm}$, $d = 10.5\,\mathrm{mm}$) with a power module of $\Delta x = 24\,\mathrm{mm}$ ($\Delta x/a = 0.214$), $\Delta y = 34\,\mathrm{mm}$ and $Q = 50\,\mathrm{W}$. The curve is derived analytically from (2)–(9) and/or (10). The thermal conductivity of the extruded aluminium heat sink is $k = 205\,\mathrm{W/mK}$. The temperature $\Delta T = T_{PN} - T_a = 10.78°\mathrm{C}$ is derived from a stationary CFD-simulation (by ICEPAK) of the heat sink shown in Fig. 1.

The heat transfer coefficient h derived this way is dependent on the heat sink fin geometry, the fan characteristic and the air-flow. It is not dependent on the power module and, therefore, characterizes the cooling of the heat sink in a very general way. The simplified thermal heat sink model with h = const at the bottom surface as employed here, does not take into account the airflow direction which distorts the temperature field (see Fig. 1(a)). In spite of these shortcomings, employing a constant value of h is justified for many different heat sink types as shown in the following sections.

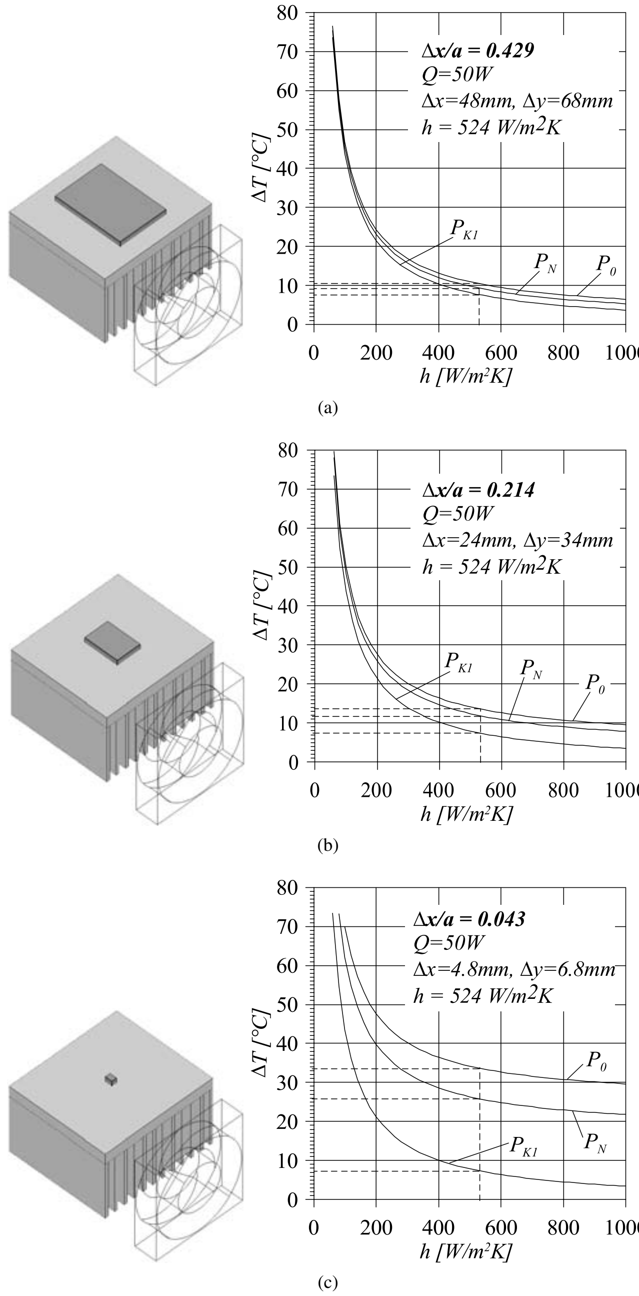

Fig. 3. Centered test heat sources of different size (characterized by $\Delta x/a$-ratio) result in different temperature measurements at selected points P_0, P_N, P_{K1} on the heat sink with $a = 112\,\mathrm{mm}$, $b = 100\,\mathrm{mm}$, $d = 10\,\mathrm{mm}$, $k = 205\,\mathrm{W/mK}$ (see Fig. 1(b)). The heat transfer coefficient h describes only the convection cooling of the heat sink via the fins and is, therefore, not affected by the test heat source geometry.

2.2 Parameter-Sensitivity Dependent on the Point of Stationary Temperature Measurement If the proposed method is to be employed in a practical design, it is essential to make sure that the mathematical method to derive the average heat transfer coefficient shows robustness against measurement inaccuracies. Fig. 3 shows the graphical method as demonstrated in Fig. 2 for different test heat source geometries and for different points of measurement at the heat sink surface. The heat transfer coefficient h is not dependent on the heat source geometry. The procedure how to derive h from the curves shown in Fig. 3 is given in detail in the text below Fig. 2.

Generally, since the temperature distribution $T(x, y, z)$-T_a is proportional to the power Q as can be directly seen from (2)–(9), the accuracy of the measurement of h can be increased by simply increasing the thermal power Q. Thermocouples that are typically available in a power electronics laboratory show absolute errors in the range of ±0.5°C. Practical limits of increasing the heating power are set by the maximum temperatures of the employed measurement equipment.

The center of the test heat source (P_0) shows the maximum temperature of the whole experimental arrangement which is difficult to measure. A hole has to be drilled into the heat sink base plate directly below the test heat source to insert the thermocouple. Alternatively, a temperature sensor must be integrated into the test heat source. Both methods change the temperature field, distort the temperature measurement and result in an increased temperature measurement error as discussed in detail in section 3.

The proposed method offers the significant advantage to measure the stationary temperature at any point of the heat sink base plate. Therefore, measuring the temperature close to the test heat source (point P_N in Fig. 1) will give an absolute temperature close to the maximum temperature occurring at the center of the test heat source, but will be easy and accurate to measure by simply pressing the thermocouple at point P_N against the heat sink surface. For larger test heat sources (larger $\Delta x/a$-ratios, see Fig. 3(a)) the temperature at P_N is much closer to the maximum center point temperature at P_0 as compared to very small test heat sources (Fig. 3(c)). This makes large test heat sources generally more attractive for this kind of measurement.

Concerning the accuracy of the value of h, dT/dh of the curves in Fig. 2 and/or Fig. 3 should be as large as possible. As shown in Fig. 4, the derivative is independent from the size of the test heat source and the point of temperature measurement, and proportional to the heating power Q [W]. Fig. 4 is based on the analytical model of the heat sink as described by (2)–(9). With a real heat sink, setting h constant is an approximation that sometimes does not work well at points P_{K1} or P_{K2} (Fig. 1) at the edge of the base plate (see also section 3). It is, therefore, also under this aspect preferable to measure the temperature close to the heat sink at a point P_N.

According to Fig. 4, for the given heat sink and heating power Q = 50 W the value of h = 524 W/m^{2}K results in $dT/dh \approx -0.016$ (m^{2}K^2)/W. This means that with an absolute temperature measurement error of, e.g., ΔT = ±0.5° at any base plate point, the value of the calculated heat transfer coefficient h for the heat sink model will vary by about Δh = ±31 W/m^{2}K. Doubling the heating power Q will increase dT/dh to −0.032 (m^{2}K^2)/W and reduce the error of the heat transfer coefficient Δh accordingly by a factor of 2.

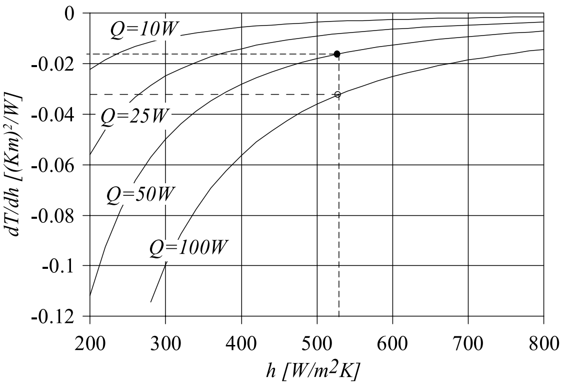

Fig. 4. The derivative dT/dh of the heat sink surface temperature dependent on the heat transfer coefficient h and the heating power Q [W]. These curves are independent from $\Delta x/a$-ratios of the test heat source and also independent from the heat sink surface point of the stationary measurement. The curve of dT/dh for Q = 50 W shown here is valid for all curves of Fig. 3.

For larger values of h, the procedure becomes obviously more and more sensitive to temperature measurement errors (see Fig. 2, 3, 4). It is very interesting to note, that with increasing value of h, the proposed heat sink model becomes more and more insensitive against errors in h because the thermal resistance of the convection $R_{th,sink-air} = \Delta T/Q \sim h^{-1}$, see (1), becomes small against the thermal resistance of the plate $R_{th,HeatSource-SinkBottom}$. Therefore, temperature measurement errors due to a flat dT/dh-curve at high h-values have only minor impact on the proposed heat sink model.

3. Calculating Thermal Step Responses Based on the Proposed Heat Sink Model

3.1 Example I: Hollow-Fin Cooling Aggregate The proposed procedure will be experimentally tested employing a hollow-fin cooling aggregate Ref. (20) as shown in Fig. 5. Assuming that the size and location of the power modules of the final system design is not known yet, a simplified heat sink model has to be set up first as described in detail in section 2. A test heat source (100 W-resistor on a 8 mm copper heat spreader) is mounted onto the center of the heat sink. After heating up and reaching steady state, the temperature on the heat sink surface close to the copper block (e.g., point P_N in Fig. 1(b)) is measured. Since the fan is in full operation, the measurement describes the forced convection air cooling as it will be employed in the final system design. If the operating environment of the heat sink in the final system (e.g., distorted air flow inside the housing) is already known, the accuracy of the whole modeling scheme can be increased by performing the measurement in a comparable environment.

One stationary temperature measurement at just one base plate surface point is sufficient to calculate the heat transfer coefficient h employing the procedure described in section 2. For testing purpose, the temperature was measured at six different points P_0, P_{N1}, P_{N2}, P_{N3}, P_{K1} and P_{K2} as shown in Fig. 6. Employing (10) and/or Fig. 2 we get the values of h as

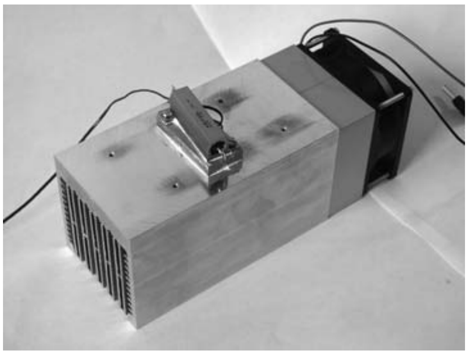

Fig. 5. Hollow-fin cooling aggregate ($150 \times 80 \times 80\,\mathrm{mm}^3$, 10.5 mm base plate thickness, aluminium with $k = 205\,\mathrm{W/mK}$) with fan. A test heat source of $Q = 100\,\mathrm{W}$ is mounted onto the center. The shown wire is connected to a thermocouple inserted in the copper-heat spreader below the heating resistor to measure the center point temperature (P_0 in Fig. 1). The heating resistor is not connected to a voltage source yet.

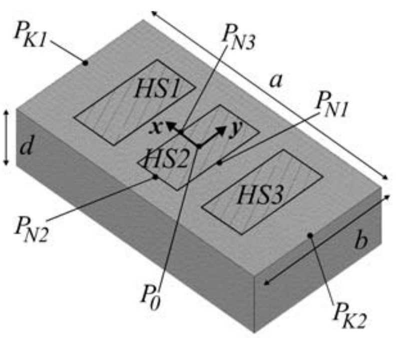

Fig. 6. Simplified thermal heat sink model of the hollow-fin cooling aggregate (Fig. 5) according to Fig. 1(b) with $h = 650\,\mathrm{W/m^2K}$ and $d = 36\,\mathrm{mm}$, $a = 150\,\mathrm{mm}$, $b = 80\,\mathrm{mm}$, $k = 205\,\mathrm{W/mK}$. In the FEM simulation the bottom wall is defined employing a Neumann boundary condition with $h = 650\,\mathrm{W/m^2}\,K = \mathrm{const}$, all other walls are defined as thermally isolating. The heat sources are modeled as 2D-elements with continuous heat distribution.

given in Table 1. The ambient temperature is $T_a = 24°\mathrm{C}$ and the heating power is $Q = 100\,\mathrm{W}$.

Ideally, all values of h should be equal. The simplified heat sink model (Fig. 1(b)) does not take into account air flow direction. Since the air is heating up along the fins, the heat sink temperature must generally rise along the x-direction (air flow direction in this example). This is why the measured temperature at P_{N3} is higher than temperature at P_{N1} or P_{N2}. Accordingly, the heat sink coefficient calculated from a P_{N3}-measurement must be lower. The same is true for P_{K1} and P_{K2}. The measurement at the center point P_0 has been performed with a thermocouple inserted into a hole drilled into the copper heat spreader of the test heat source. While temperature measurements at all other points are performed by simply pressing the thermocouple onto the base plate surface, performing a P_0-measurement provides additional thermal resistances of the copper block and of the thermal grease between heat sink and copper block ($\lambda = 1.0\,\mathrm{W/mK}$, thickness $d_G = 30\,\mu\mathrm{m}$). This additional thermal resistance increases the measured temperature at P_0 by about 4.5°C resulting in

Table 1. Coordinates (x is in air flow direction), measured temperatures and resulting heat transfer coefficients for different points at the heat sink surface. Further parameters are $d = 36\,\mathrm{mm}$, $a = 150\,\mathrm{mm}$, $b = 80\,\mathrm{mm}$, $\Delta x = 25\,\mathrm{mm}$, $\Delta y = 53\,\mathrm{mm}$, $k = 205\,\mathrm{W/mK}$. Note that the coordinates given here according to the coordinate system in Fig. 6 are different from the coordinate system of Fig. 1(b) which has to be employed if working with equations (2)–(9).

point	*coordinate x [mm]*	*coordinate y [mm]*	*T [°C] measured*	*h [W/m²K] from (10)*
P_0	0	0	44	620
P_{N1}	-12.5	0	41	670
P_{N2}	0	-26.5	41	650
P_{N3}	+12.5	0	42	620
P_{K1}	+75	0	34	830
P_{K2}	-75	0	33	920

an inaccurately reduced value of h. The properties of the thermal grease where derived by comparing the stationary experimental measurement to a FEM simulation and are in good accordance with values typically given in datasheets. To set up the simplified thermal model of the hollow-fin cooling aggregate, the average value of h from the points P_{N1}, P_{N2}, and P_{N3} is formed as approximately

$$h = 650\,\frac{\mathrm{W}}{\mathrm{m^2K}} \quad\cdots\cdots(11)$$

The simplified thermal model of the hollow-fin cooling aggregate consists of an aluminium block with the heat sources mounted onto it as shown in Fig. 6. Now location, size and number of the power modules of the planned system design have to be defined in order to proceed with the modeling.

The thickness of this block is not equal to the base plate of the heat sink but has to take into account the fins. The fins typically provide significant mass that acts as thermal capacitance and, therefore, have a strong influence on the thermal time constants of the heat sink. Furthermore, before the heat can flow from the heat sink into the cooling air, the heat has to flow partly through the fins, which increases the thermal resistance of the heat sink. The fins also increase the thermal coupling of two heat sources mounted onto the heat sink in cases where the heat sources are mounted above the same fins. Therefore, the fins have to be considered in form of an increase of the thickness d of the simplified model.

The base plate mass of the hollow-fin cooling aggregate is

$$m_{BP} = (0.150 \cdot 0.080 \cdot 0.0105)\mathrm{m}^3 \cdot 2800\,\frac{\mathrm{kg}}{\mathrm{m}^3} = 0.353\,\mathrm{kg} \quad\cdots\cdots(12)$$

Since the total mass of the heat sink was measured as 1.206 kg, the thickness of the simplified model in Fig. 6 has to be by a factor of 3.42 higher than the base plate thickness resulting in

$$d = 36\,\mathrm{mm} \quad\cdots\cdots(13)$$

Based on the simplified thermal heat sink model of Fig. 6, the thermal step responses of the various power modules located there have to be found. This can most effectively be done by a transient numerical temperature field simulation. We currently employ commercial 3D-FEM software (ICEPAK) where we have to solve only the heat conduction equation because there are no fluids in the model of Fig. 6. Instead of simulating the air flow where the simulator has to solve five differential equations (mass conservation, energy conservation, impulse conservation in vector form) simultaneously, we now have only one differential equation to solve (heat conduction equation = energy conservation). Also, the very complex meshing of the fins and the channels between the fins is avoided. Therefore, the simulation time of the transient step response is reduced from more than one hour for a full scale CFD (computational fluid dynamics) simulation to 20 seconds for the simplified model shown in Fig. 6. What is even more important is that this very fast simulation shows excellent numerical convergence while the CFD simulation tends to be numerically unstable and/or gives inaccurate results.

Alternatively to employing FEM software, much easier to program finite difference methods (FDM) will give accurate results especially due to the simple geometry of the simplified heat sink model (only one homogenous block with homogenous boundary conditions and rectangular 2D heat sources). Since we are working on automating the modeling procedure described in this paper, we will implement an according FDM code as it is well known from the literature Ref. (21). Writing CFD code for such a project would increase the complexity of the software, the time effort and the workload on an unrealistically large scale.

In order to validate the procedure experimentally the setup of Fig. 6 is realized as shown in Fig. 7 and experimental results are given in Fig. 8 (connected dots). Results of the simulated (FEM) thermal step response from Fig. 6 are shown in Fig. 8 as solid lines. The measured temperatures of the thermocouples have been corrected according to the additional temperature drop caused by the thermal resistance of copper block and thermal grease.

The thermal step response of the heat source that is heating up (e.g., $HS1$ in Fig. 8(a), $HS2$ in Fig. 8(b) and $HS3$ in Fig. 8(c)) is always distorted in the time range below about one minute. This effect indicates an additional thermal capacitance close to the active heat source, which comes from

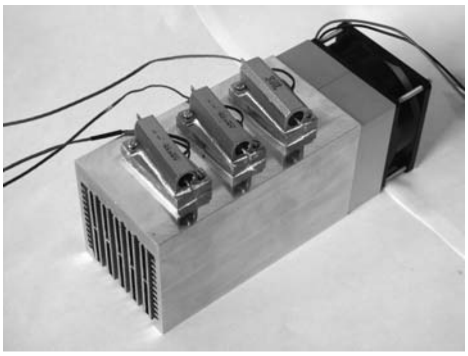

Fig. 7. For testing the theory, three 100 W-heat sources are mounted onto the heat sink. Each heat source consists of a heating resistor on a $25 \times 53\,\mathrm{mm}^2$ copper heat spreader of 8 mm thickness containing a 1.5 mm diameter hole with an inserted thermocouple for temperature measurement. The heat sources are labeled $HS1$, $HS2$, and $HS3$ from the left to the right (opposite direction of the airflow, see also Fig. 6). The space between two neighbor heat sources is 15 mm.

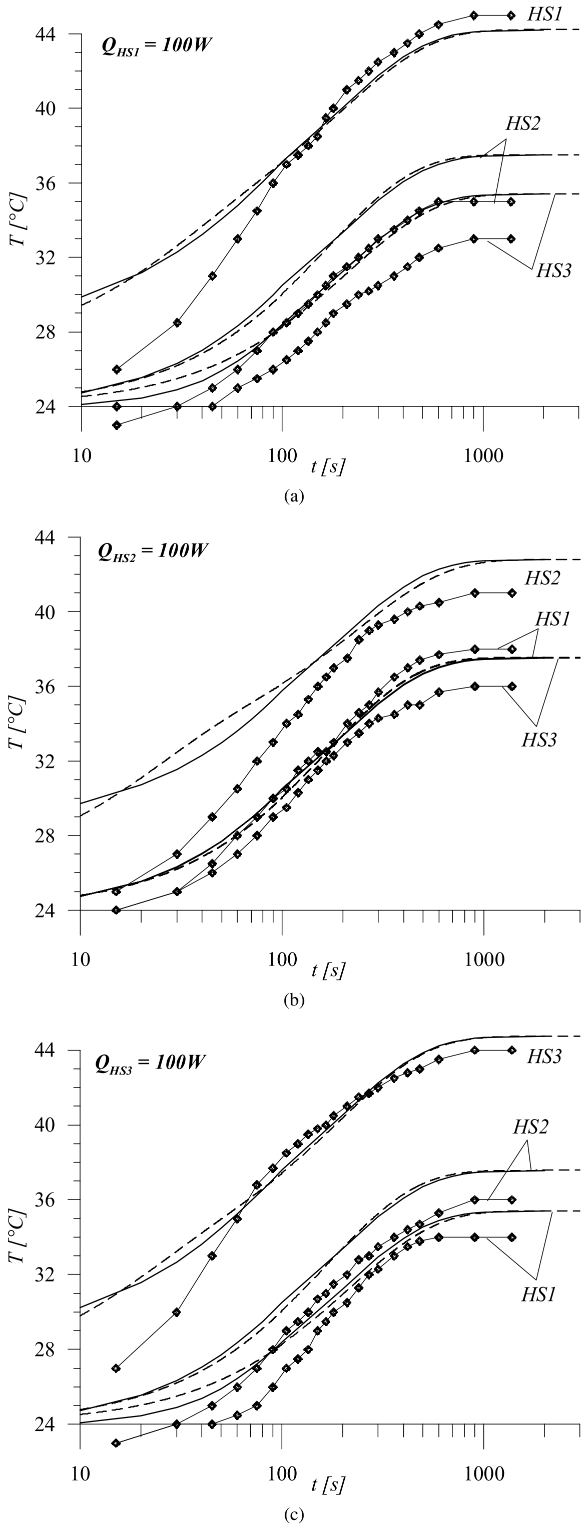

Fig. 8. Thermal step responses of all three heat sources $HS1$, $HS2$ and $HS3$ for heating (a) only $HS1$ with Q = 100 W, (b) only $HS2$ with Q = 100 W and (c) only $HS3$ with Q = 100 W. The connected dots are experimentally measured, the solid lines are resulting from transient FEM simulations of the simplified heat sink model. The dashed lines are resulting from the RC thermal equivalent network model as described in section 4 and in Table 2.

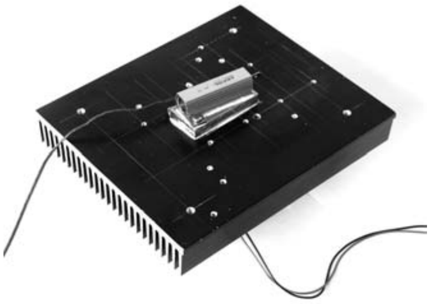

Fig. 9. Extruded heat sink ($150 \times 177 \times 26.5\,\mathrm{mm}^3$, 5 mm base plate thickness, aluminium with $k = 205\,\mathrm{W/Km}$) with a fan mounted onto the bottom side (only the wires of the fan are visible in the photo). A test heat source of $Q = 100\,\mathrm{W}$ is mounted onto the center. The shown wire is connected to a thermocouple inserted in the copper-heat spreader below the heating resistor to measure the center point temperature (P_0 in Fig. 6).

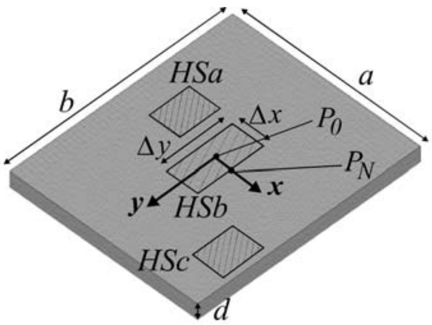

Fig. 10. Simplified thermal heat sink model of the extruded heat sink (Fig. 9) with $h = 220\,\mathrm{W/m^2K}$, $d = 12.7\,\mathrm{mm}$, $a = 150\,\mathrm{mm}$, $b = 177\,\mathrm{mm}$, $k = 205\,\mathrm{W/mK}$. 2D heat sources are sized and located as described in Fig. 11.

the heating resistor and partly from the copper heat spreader (both not covered by the simplified model of Fig. 6).

Employing flat heat sources, e.g. power semiconductor chips, would result in more accurate transient measurements. This has, however, no relevance for setting up our simplified thermal heat sink model, because this is based on a stationary temperature measurement directly on the heat sink base plate surface close to the test heat source but not inside the copper heat spreader.

The temperature errors of the simplified heat sink model are below 10% compared to the experimental results in Fig. 8 for the temperature rise of the single heat source that is being heated up. The errors of the temperature increases of the other two heat sources due to thermal coupling are larger (up to 20%) but the model always predicts higher temperatures from thermal coupling effects, which guarantees a safety margin in the thermal design process. The reason for this always higher temperature prediction for thermal coupling is that the heat flows not only through the base plate but also through the fins. In the proposed simplified thermal model the fin material is employed to increase the thickness d of the model plate. In reality, fins have an orientation and conduct heat only in one direction in an effective way. This effect can be considered in the simplified model (Fig. 6) by making conductivity k dependent on the direction.

3.2 Example II: Extruded Heat Sink As another example, an extruded heat sink (Fig. 9) is tested experimentally in analogy to the previous section. Compared to the hollow-fin cooling aggregate, the air flow is directed from the fan at the bottom side directly against fins and base plate which results in a more non-homogenous cooling effect and, therefore, also in a more non-homogenous heat transfer coefficient. Furthermore, the base plate is thinner compared to its length and/or width. In spite of this, the simplified model assuming $h = \mathrm{const}$ gives accurate results also for this heat sink as will be shown in the following.

From stationary temperature measurements at the base plate close to the centered test heat source (e.g. P_N in Fig. 10), we receive for the characteristic heat transfer coefficient of this heat sink (with parameters $d = 12.7\,\mathrm{mm}$, $a = 150\,\mathrm{mm}$, $b = 177\,\mathrm{mm}$, $\Delta x = 25\,\mathrm{mm}$, $\Delta y = 53\,\mathrm{mm}$, $k = 205\,\mathrm{W/mK}$)

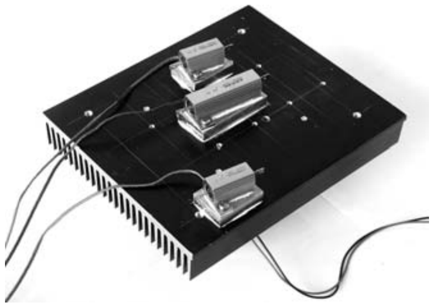

Fig. 11. For testing the theory, three different heat sources are mounted onto the heat sink. The heat sources are labeled *HSa*, *HSb*, and *HSc* from the back to the front (see Fig. 10). The center point coordinates of these three heat sources are *HSa* (−38.5 mm/−14 mm), *HSb* (0/0) and *HSc* (57.5 mm/47 mm). Each heat source consists of a heating resistor on a copper heat spreader of 8 mm thickness containing a 1.5 mm diameter hole with inserted thermocouple. *HSa* and *HSc* (both emitting 55 W thermal power) have a $33 \times 25\,\mathrm{mm}^2$ heat spreader area, *HSc* (75 W) has a heat spreader area of $53 \times 25\,\mathrm{mm}^2$. Note that the coordinate system employed here and also shown in Fig. 10 is different to the coordinate system of Fig. 1(a) that has to be employed if (2)–(9) are used.

$$h = 220 \frac{\mathrm{W}}{\mathrm{m^2K}} \quad \cdots\cdots (14)$$

to be employed as boundary condition in the simplified heat sink model (Fig. 10). The base plate thickness of 5 mm has to be increase by a factor 2.54 to take into account the mass of the fins resulting in $d = 12.7\,\mathrm{mm}$ for the simplified model. In Fig. 10 a test arrangement of three different heat sources is set up to be tested against the results of the experimental setup shown in Fig. 11.

The experimental results of the thermal step responses (connected dots in Fig. 12) are in good agreement with the results from the transient numerical simulation of the simplified heat sink model (solid lines).

4. Thermal Equivalent Circuit of the Heat Sink Based on the Impedance Matrix Model

One way to set up a simple equivalent thermal network model based on the heat conduction equation is employing the impedance matrix method Ref. (13). The underlying mathematical principle is superposition of different heat sources assuming a linear differential equation. Strictly

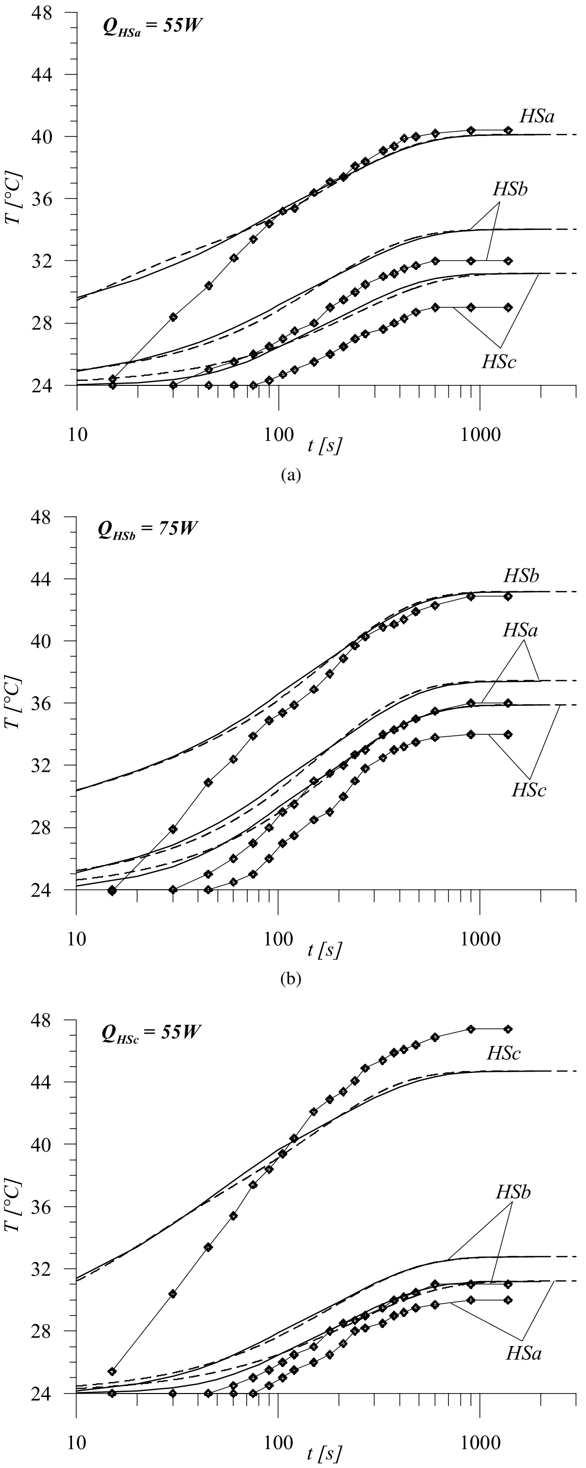

Fig. 12. Thermal step responses of all three heat sources *HSa*, *HSb* and *HSc* for heating (a) only *HSa* with Q = 55 W, (b) only *HSb* with Q = 75 W and (c) only *HSc* with Q = 55 W. The dots are experimentally measured, and the solid lines are resulting from the transient FEM simulation of the simplified heat sink model. The dashed lines are resulting from the RC thermal equivalent network model as described in section 4 and in Table 3.

speaking, the heat conduction equation is not a linear differential equation because properties like thermal conductivity and thermal capacity are temperature dependent. Since this dependency is not very strong within temperature ranges as typically found in power electronic operating ranges, applying superposition is justified in most cases.

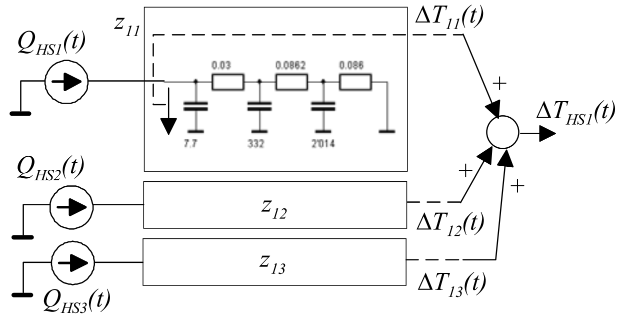

Fig. 13. General scheme of the RC thermal equivalent network of a heat sink with three power modules mounted onto the base plate. In this figure only the network representing the temperature formation of power module $HS\,1$ is shown. Each current source represents the total losses (thermal power) of one power module. The RC-circuits in the boxes are modeled according to the thermal step responses derived via transient FEM simulation of the simplified heat sink model. In Table 2 and Table 3 implementations of $z_{ji}(t)$ for both experimental heat sinks of section 3 are given.

Each heat source has to be heated up, and the temperature rise (thermal step response) of this heat source, but also of all other heat sources, has to be measured (see Fig. 8 and Fig. 12). In the following, we will write $z_{AB}(t)$ to indicate that heating up heat source B will have an effect on the temperature of the heat source located at A as described by the transient thermal impedance $z_{AB}(t)$. Since each of n heat sources mounted onto a heat sink influences the temperatures of all other heat sources, the total number of thermal step responses to be recorded or calculated is n^2. The scheme can be described by a matrix equation as

$$\begin{pmatrix}\Delta T_{HS\,1}\\ \Delta T_{HS\,2}\\ \Delta T_{HS\,3}\end{pmatrix} = \begin{pmatrix} z_{11}(t) & z_{12}(t) & z_{13}(t)\\ z_{21}(t) & z_{22}(t) & z_{23}(t)\\ z_{31}(t) & z_{32}(t) & z_{33}(t)\end{pmatrix}\cdot\begin{pmatrix}Q_1\\ Q_2\\ Q_3\end{pmatrix}\cdots\cdots\cdots(15)$$

in case of the hollow-fin cooling aggregate of section 3.1.

Here, the thermal impedance $z_{11}(t)$ is the normalized (divided through the thermal power $Q_{HS\,1}$) thermal step response of $HS\,1$ in Fig. 8(a), where $HS\,1$ is heated up with $Q_{HS\,1}$ = 100 W. The step response of $HS\,2$ in the same figure would give after normalization (dividing through $Q_{HS\,1}$) the transient thermal impedance $z_{21}(t)$, and so on. Fig. 13 shows how to implement the matrix equation in a circuit simulator. Thermal power emitted from the power modules is modeled as current provided by signal-controlled current sources $Q_{HS\,i}(t)$, and the transient thermal impedances $z_{ji}(t)$are modeled as RC-circuits. The voltage at the input side of such a RC-circuit represents the partial temperature rise $\Delta T_{ji}(t)$ caused by a heat source *HSi*. Due to the principal of superposition all partial temperatures $\Delta T_{ji}(t)$ must be added to form the temperature rise $\Delta T_{HS\,j}(t)$ of the module case (at its center) compared to ambient.

The impedance matrix grows with the square of the number of power modules. In this example there are 9 matrix entries for just three power modules. For a larger number of power modules on one heat sink, the number of necessary RC-representations modeling the matrix entries grows quickly and will increasingly slow down the circuit simulation. It is, therefore, essential to keep the number of single RC-cells of each matrix entry as low as possible.

There are widely used and well known procedures to extract RC-equivalent circuits from measured or simulated thermal step responses. These methods are highly accurate but result in a large number (typically 4–10) of single RC-cells. In this paper we employed a search algorithm in order to find the optimum parameter set (R- and C-values) to fit the reference step response (FEM-simulation from the simplified heat sink model, solid lines in Fig. 8 and Fig. 12) with minimum error for a given structure and cell number. For a given three-cell Cauer circuit, the search algorithm found the parameter values as given in Fig. 14 for the transient thermal impedance $z_{11}(t)$ from section 3.1. Network structures and parameter values for all 18 thermal step responses calculated and measured in section 3 are given in Table 2 and Table 3. Thermal step responses of these RC-networks are shown in Fig. 8 and Fig. 12 as dashed lines and are in very good agreement with the FEM-simulation (solid lines). Increasing the RC-cell number of the single matrix entries would eliminate the very small remaining inaccuracies but this would not make much sense because of the general inaccuracies of the simplified heat sink model in the range of 5–10%.

The representation of Fig. 14 is based on mathematical curve fitting and provides a partial temperature that does not exist in reality. It is a mathematical model with no real physical meaning (although it is a Cauer-type equivalent circuit).

For symmetry reasons there is always $z_{AB}(t) = z_{BA}(t)$ which reduces the number of different matrix entries. In case of the hollow-fin cooling aggregate there is an additional

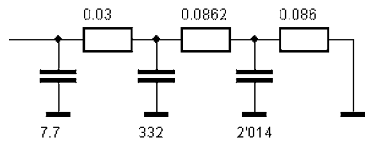

Fig. 14. Possible implementation of the transient thermal impedance $z_{11}(t)$ in a circuit simulator. With the current at the input side representing the power Q_{HS1} emitted by heat source $HS1$, the voltage drop from input side to ground represents the partial temperature rise (against ambient) $\Delta T_{11}(t) = z_{11}(t) \cdot Q_{HS1}(t)$.

Table 2. Possible entries of the impedance matrix of (15) representing the hollow-fin cooling aggregate (section 3.1). The values are found by a search algorithm, the thermal step responses are shown in Fig. 8 (dashed lines). They are in very good agreement with the reference curves from the FEM-simulation of the simplified thermal heat sink (solid lines in Fig. 8).

$Z_{11}(t) = Z_{33}(t)$ 0.03 0.0862 0.086 7.7 332 2'014	**$Z_{12}(t) = Z_{21}(t) = Z_{23}(t) = Z_{32}(t)$** 0.0157 0.12 1'174 98	**$Z_{13}(t) = Z_{31}(t)$** 0.014 0.1 1'812 80
$Z_{21}(t) = Z_{12}(t) = Z_{23}(t) = Z_{32}(t)$ 0.0157 0.12 1'174 98	**$Z_{22}(t)$** 0.019 0.0849 0.084 3.3 251 2'591	**$Z_{23}(t) = Z_{32}(t) = Z_{12}(t) = Z_{21}(t)$** 0.0157 0.12 1'174 98
$Z_{31}(t) = Z_{13}(t)$ 0.014 0.1 1'812 80	**$Z_{32}(t) = Z_{23}(t) = Z_{12}(t) = Z_{21}(t)$** 0.0157 0.12 1'174 98	**$Z_{33}(t) = Z_{11}(t)$** 0.03 0.0862 0.086 7.7 332 2'014

Table 3. Possible entries of the impedance matrix of (15) representing the extruded heat sink (section 3.2) with values found by a search algorithm. The thermal step responses are shown in Fig. 12 and are in very good agreement with the reference curves from the FEM-simulation of the simplified thermal heat sink (solid lines in Fig. 12).

$Z_{11}(t)$ 0.034 0.117 0.1421 2.99 101 1'173	**$Z_{12}(t) = Z_{21}(t)$** 0.02 0.1602 391 624	**$Z_{13}(t) = Z_{31}(t)$** 0.0109 0.12 1'810 0.6
$Z_{21}(t) = Z_{12}(t)$ 0.02 0.1602 391 624	**$Z_{22}(t)$** 0.071 0.053 0.1336 24 353 881	**$Z_{23}(t) = Z_{32}(t)$** 0.01 0.1495 1'172 0.9
$Z_{31}(t) = Z_{13}(t)$ 0.0109 0.12 1'810 0.6	**$Z_{32}(t) = Z_{23}(t)$** 0.01 0.1495 1'172 0.9	**$Z_{33}(t)$** 0.076 0.15 0.15 10 116 889

geometric symmetry between $HS\,1$ and $HS\,3$ that further reduces the number of different matrix entries.

The network shown in Fig. 13 calculates temperature differences $\Delta T_{HS\,i}$ from the heat sink below the power module $HS\,i$ to ambient temperature T_a. The temperatures $T_a + \Delta T_{HS\,i}$ represent the heat sink temperature (realized in the circuit simulation in form of voltage-controlled voltage-sources) for the thermal model of the power semiconductor that is independently modeled in the circuit simulator. Again, the underlying principle is superposition and one can directly numerically calculate the power semiconductor junction temperatures under consideration of the thermal behavior of the heat sink. Generally, the thermal models of semiconductor (including thermal grease) and heat sink have to be coupled via signal-controlled current- and voltage sources, but must not be coupled directly when applying the impedance matrix.

5. Conclusion

The paper proposes a general RC thermal equivalent network model of a heat sink to be easily embedded in any circuit simulator. The network model considers convection cooling, thermal hotspots below the power modules, thermal time constants introduced by the heat sink, and thermal coupling between different power modules mounted onto the base plate. Experiments for two different heat sinks show temperature errors below 10%.

The proposed procedure is complex but can easily be automated in form of software. Currently such a software tool is under development at the Power Electronic Systems Laboratory, ETH Zurich. The input to this package is the heat sink geometry and one stationary temperature measurement. The output will be the thermal RC equivalent circuit ready for embedding in any circuit simulation. The whole computational effort of the proposed modeling procedure should be in the range of just a few minutes.

(Manuscript received May 6, 2005,
revised Feb. 6, 2006)

References

(1) U. Drofenik and J.W. Kolar: "Thermal Analysis of a Multi-Chip Si/SiC-Power Module for Realization of a Bridge Leg of a 10kW Vienna Rectifier", Proc. of the 25th IEEE Int. Telecommun. Energy Conference, pp.826–833, Yokohama, Japan (2003-10)

(2) U. Drofenik and J.W. Kolar: "A General Scheme for Calculating Switching- and Conduction-Losses of Power Semiconductors in Numerical Circuit Simulations of Power Electronic Systems", Proc. of the 5th Int. Power Electron. Conference, Niigata, Japan (2005-4)

(3) D. Boroyevich and J.Z. Chen: "Integrated Multidisciplinary Modeling, Analysis and Design in Power Electronics", Proc. of the 2003 CPES Annual Seminar, Blacksburg, USA (2003-4)

(4) J.Z. Chen, Y. Wu, D. Borojevich, and J.H. Bohn: "Integrated Electrical and Thermal Modelling and Analysis of IPEMs", Proc. of the 16th IEEE Applied Power Electron. Conference, Anaheim, USA (2001-3)

(5) C.-S. Yun: "Static and Dynamic Thermal Behavior of IGBT Power Modules", Series in Microelectronics, Vol.124, Dissertation ETH No.13784 (2001)

(6) O. Karim, J.-C. Crebier, C. Gillot, C. Schaeffer, B. Mallet, and E. Gimet: "Heat Transfer Coefficient for Water Cooled Heat Sink: Application for Standard Power Modules Cooling at High Temperature", Proc. of the 32nd Power Electron. Specialists Conference, Vancouver, Canada (2001-6)

(7) O. Karim, C. Schaeffer, B. Mallet, M. Coyaud, and E. Gimet: "Power Module Integrated Cooling Design Using CFD Simulation", Conference Record of the 2001 IEEE, Conference 36th IAS Annual Meeting, Vol.3, pp.1925–1930, Chicago, USA (2001-9)

(8) P. Vales and J.-M. Dorkel: "Electrothermal Simulation of Fast Switching Integrated Power Electronics Circuits", Proc. of the 7th European Conference on Power Electron. and Appl., Vol.4, pp.4.151–4.156, Trondheim, Norway (1997-9)

(9) J.J. Rodriguez, Z. Parilla, M. Velez-Reyes, A. Hefner, D. Berning, J. Reichl, and J. Lai: "Thermal Component Models for Electro Thermal Analysis of Multichip Power Modules", Proc. of the 2003 CPES Annual Seminar, Blacksburg, USA (2003-4)

(10) M. Bikdash, H. Rayadurgam, Y. Pang, and E. Scott: "Algorithm to Determine the Topology of a Thermal Equivalent Circuit from Simulation Data", Proc. of the 2003 CPES Annual Seminar/Industry Review, Blacksburg, USA (2003-4)

(11) V. Szekely and M. Rencz: "Increasing the Accuracy of Thermal Transient Measurements", *IEEE Trans. Components* & *Packaging Tech.*, Vol.25, No.4 (2002-11)

(12) A. Aranyosi, A. Ortega, R.A. Griffin, S. West, and D.R. Edwards: "Compact Thermal Models of Packages Used in Conduction Cooled Applications", *IEEE Trans. Components* & *Packaging Tech.*, Vol.23, No.3 (2000-9)

(13) T. Franke, G. Zaiser, J. Otto, M. Honsberg-Riedl, and R. Sommer: "Current and Temperature Distribution in Multi-Chip Modules under Inverter Operation", Proc. of the 8th European Conference on Power Electron. and Appl., Lausanne, Switzerland (1999)

(14) O. Schepp and M. Lenz: "A Versatile Electrothermal Model of an Integrated Full Bridge Device Taking into Account Various Boundary Conditions", Proc. of the 12th IEEE Appl. Power Electron. Conference, Vol.1, pp.185–190, Atlanta, USA (1997-2)

(15) L.L. Rouve, C. Schaeffer, and E. Farjah: "Thermal Behavior of IGBT Subjected to Short Power Pulses of High Amplitude", Proc. of the 9th IEEE Appl. Power Electron. Conference, Vol.1, pp.487–492, Orlando, USA (1994-2)

(16) C. Schaeffer, J.-P. Ferrieux, and R. Perret: "Thermal Simulation in Power Electronics", Proc. of the 7th IEEE Applied Power Electronics Conference, pp.780–784, Boston, USA (1992-2)

(17) C. Lasance: "The Influence of Various Common Assumptions on the Boundary-Condition-Independence of Compact Thermal Models", *IEEE Trans. on Components and Packaging Tech.*, Vol.27, No.3, pp.523–529 (2004-9)

(18) B. Jaeschke and H. Mecke: "Method for Calculating the Static and Dynamic Behavior of Large Heat Sinks with Temperature Dependent Heat Sources", Proc. of the 47th European Power Electron. Conference, pp.441–447, Nuremberg, Germany (2003-5)

(19) G.N. Ellison: "Maximum Thermal Spreading Resistance for Rectangular Sources and Plates With Nonunity Aspect Ratios", *IEEE Trans. on Components and Packaging Tech.*, Vol.26, No.2, pp.439–454 (2003-6)

(20) E.G. Fischer: "Extruded heatsinks: SK 121", datasheet http://www.fischerelektronik.de/fischer/upload/Fischer/A023.pdf

(21) S.V. Patankar: Numerical Heat Transfer and Fluid Flow, ISBN 0-89116-522-3, Taylor & Francis (1980)

Uwe Drofenik (Non-member) was born in Moedling, Austria, in 1970. He received the M.Sc. degree (cum laude) and also the Ph.D. degree (cum laude) in electrical engineering from the Vienna University of Technology, Austria, in 1995 and 1999, respectively. He is currently performing scientific research and teaching at the Swiss Federal Institute of Technology (ETH) Zurich. In 1996 he was a researcher at the Masada-Ohsaki Laboratory at the University of Tokyo, Japan. His research interests include thermal analysis and design of power systems, power factor correction, numerical simulation and Java programming. He has published more than 40 conference and journal papers, and received the Isao Takahashi Power Electronics Award of the IEE Japan in 2005. Uwe Drofenik is member of the Austrian Society of Electrical Engineering (OVE) and of IEEE.

Johann W. Kolar (Member) studied industrial electronics at the University of Technology Vienna, Austria, where he also received the Ph.D. degree (summa cum laude). From 1984 to 2001 he was with the University of Technology in Vienna, where he was teaching and working in research in close collaboration with the industry in the fields of high performance drives, high frequency inverter systems for process technology and uninterruptible power supplies. He has proposed numerous novel converter topologies, e.g., the VIENNA Rectifier and the Three-Phase AC-AC Sparse Matrix Converter concept. Dr. Kolar has published over 150 scientific papers in international journals and conference proceedings and has filed more than 50 patents. He was appointed Professor and Head of the Power Electronics Systems Laboratory at the Swiss Federal Institute of Technology (ETH) Zurich on Feb. 1, 2001. The focus of his current research is on novel AC-AC and AC-DC converter topologies with low effects on the mains for telecommunication systems, More-Electric-Aircraft applications and distributed power systems utilizing fuel cells. A further main area of research is the realization of ultra-compact intelligent converter modules employing latest power semiconductor technology (SiC) and novel concepts for cooling and EMI filtering. Dr. Kolar is a Senior Member of the IEEE and a member of the IEEJ and of Technical Program Committees of numerous international conferences in the field. From 1997 through 2000 he served as an Associate Editor of the IEEE Trans. on Industrial Electronics and since 2001 as an Associate Editor of the IEEE Trans. on Power Electronics.